



CHORUS

This is the accepted manuscript made available via CHORUS. The article has been published as:

Sequential insulator-metal-insulator phase transitions of VO_2 triggered by hydrogen doping

Shi Chen, Zhaowu Wang, Lele Fan, Yuliang Chen, Hui Ren, Heng Ji, Douglas Natelson, Yingying Huang, Jun Jiang, and Chongwen Zou

Phys. Rev. B **96**, 125130 — Published 18 September 2017

DOI: [10.1103/PhysRevB.96.125130](https://doi.org/10.1103/PhysRevB.96.125130)

Sequential Insulator-Metal-Insulator Phase Transitions of VO₂ Triggered by Hydrogen Doping

Shi Chen¹⁺, Zhaowu Wang^{2,3+}, Lele Fan¹, Yuliang Chen¹, Hui Ren¹, Heng Ji⁴,
Douglas Natelson⁴, Yingying Huang⁵, Jun Jiang^{2*}, Chongwen Zou^{1*}

¹National Synchrotron Radiation Laboratory, University of Science and Technology of China, Hefei, 230029, China.

² Hefei National Laboratory for Physical Sciences at the Microscale, iChEM (Collaborative Innovation Center of Chemistry for Energy Materials), Hefei Science Center (CAS), and School of Chemistry and Materials Science, University of Science and Technology of China, Hefei, 230026, China.

³ School of Physics and Engineering, Henan University of Science and Technology, Luoyang, Henan 471023, P. R. China

⁴Department of Physics and Astronomy, MS 61, Rice University, 6100 Main Street, Houston, Texas 77005, United States

⁵School of Physics and Optoelectronic Technology and College of Advanced Science and Technology, Dalian University of Technology, Dalian 116024, China

Corresponding Authors: jiangjl@ustc.edu.cn ; czou@ustc.edu.cn

+These two authors contributed equally to this paper.

Abstract

As a typical correlated oxide, VO₂ has attracted significant attentions due to its pronounced thermal-driven metal-insulator transition. Regulating electronic density through electron-doping is an effective way to modulate the balance between competing phases in strongly correlated materials. However, the electron-doping triggered phase transitions in VO₂ as well as the intermediate states are not fully explored. Here, we report a controlled and reversible phase transition in VO₂ films by continuous hydrogen doping. Metallic and insulating phases are successively observed at room temperature as the doping concentration increases. The doped electrons linearly occupy *V3d-O2p* hybridized orbitals and consequently modulate the filling of the VO₂ conduction band-edge states, resulting the electron-doping driven continuous phase transitions. These results suggest the exceptional sensitivity of VO₂ electronic properties to electron concentration and orbital occupancy, providing key information for the phase transition mechanism.

Since Mott predicted the first-order metal-insulator transition (MIT) behavior several decades ago, the underlying physics of how electron-electron interactions affect electronic structures of strongly correlated systems has become a hot field of condensed matter physics. As a typical correlated oxide, monoclinic vanadium dioxide (M-VO₂) undergoes a MIT process from metal to insulating state at the critical temperature near 68°C [1,2]. This transition is believed to be driven by the Mott transition associated with electron-electron correlations [3–5] or the Peierls transition involving electron-phonon interactions [6,7], although the actual MIT mechanism is still under debate.

Regulating electronic density through atomic doping is an effective way to modulate the balance between competing phases in strongly correlated materials [8,9]. It is reported that hydrogen incorporated into M-VO₂ crystals can induce the electron doping effect and stabilize the metallic VO₂ phase at room temperature [10-14] or even lead to an insulating phase [15]. Fig. 1(a) shows both the normal temperature-triggered MIT (from insulating M-VO₂ to metallic rutile VO₂ (R-VO₂)) as well as the phase transitions driven by reversible hydrogen doping. Different from the temperature induced MIT, the metallic H-VO₂ (H-VO₂(M)) is produced by light doping concentration, while further hydrogenation treatment up to the saturation point of HVO₂ leads to a new insulating H-VO₂ (H-VO₂(I)) state at room temperature.

Explained in the context of crystal-field theory [16,17], the H-doping induced band structure evolutions is preliminarily represented in Fig. 1(b). For the pure M-VO₂ crystal, the Fermi level is located in the ~0.6eV insulating gap between the edge states of d_{//} and d_{//}*/π* orbitals. Under low H-doping treatment, the conduction band-edge states of d_{//}*/π* are partially filled, resulting in a metallic state. Upon further hydrogenation, the d_{//}* band become fully occupied, producing new valence band-edge states. This leads to a new insulating gap and an insulating H-doped VO₂ crystal. As electron-electron correlations and electron-lattice interactions are always relevant, the variation of electronic structure also influences the crystal lattice structure, such as the V-V bonds. However, largely due to the difficulties of characterizing the dynamic doping process from incompletely hydrogenated states to

the maximally H-doped state, this electron-doping triggered phase transitions including those intermediate states are scarcely studied, and thereby a clear mechanism for the doping-based transitions was still not arrived.

Here, we report in-situ synchrotron based characterizations to directly monitor the dynamics of H atom doping in VO₂ crystals. This characterization captures the lattice/charge variations as well as the electronic structure evolution during the reversible phase transitions. Based on the experimentally determined geometric details, first-principle theoretical studies show the gradual filling of conduction band-edge states with nearly linear dependence on H-doping level, which was unattainable in previous works. The underlying mechanism for the electron doping-driven insulator-metal-insulator phase transitions is thus revealed, indicating the filling-based evolution of the semiconductor conduction band-edge states to valence band-edge states.

The 50 nm M-VO₂/Al₂O₃ (0001) epitaxial films were deposited by an rf-plasma assisted oxide-MBE method [18]. Metallic H-VO₂ (M) and insulated H-VO₂ (I) films were obtained by hydrogenation for different time in Ar/15% H₂ gas mixture with Au particles as the catalyst [12, 15]. Experimental details can be found in the Supporting Information. From the in-situ R-T measurement in vacuum conditions, the insulating H-VO₂ (I) gradually became a metallic sample as shown in Fig. 1(c). This metallic state was quite stable in vacuum. Upon further annealing of this metallic H-VO₂ (M) sample in air, the material will gradually revert to its initial monoclinic structure as shown in Fig. 1(d). In fact, if conducting the R-T tests in air, the phase transformation of the hydrogenated VO₂ film from the insulating state to metallic state, and then back to the initial (monoclinic) insulator state could be observed (Fig.S1 in Ref. [19]). This suggests that the hydrogenated VO₂ film is more stable in vacuum than in the air condition.

The chemical states of the hydrogenated VO₂ were examined by X-ray photoelectron spectroscopy (XPS) in Fig. 2(a). There exists double peaks for V2p_{3/2} at 515.5eV, 516.0 eV and 517.1 eV, which are assigned to V³⁺, V⁴⁺ and V⁵⁺ states, respectively [20,21]. It can be observed that due to the electron doping, the chemical

state of V atoms is partially changed from V^{4+} to V^{3+} state. The $O1s$ peak at 530.1 eV is from vanadium oxide and the peak at 531.9 eV originates from the $-OH$ species [12,22,23]. For hydrogenated VO_2 , the $-OH$ peak is much stronger than V-O peak, indicating the formation of $-OH$ bonds [22,23]. After annealing the H- VO_2 samples in air for 30 min, the $-OH$ peak decreases substantially and the sample almost reverts to the undoped M-phase. Fig. 2(b) shows the changes of intensity ratio between the $-OH$ peak and V-O peak before and after the H-doping treatment. From these results, we can then estimate the hydrogen concentration by XPS curve fitting (Fig.S2 in Ref. [19]) and obtain the stoichiometric values of $H_{0.64}VO_2$ for the metallic H- VO_2 (M) and $H_{0.89}VO_2$ for the insulating H- VO_2 (I). Nevertheless, it is difficult to determine the exact H-atom concentration because of possible intermediate phases during experimental measurements.

The evolution of electronic structures can be inferred from measuring optical band structures. In-situ UV-Vis spectra in Fig. 2(c) indicated the enhancement of visible transparency along with the increasing H-concentration in VO_2 , suggesting the gradual filling of empty d_{xy} states at conduction band edge [24, 25]. Meanwhile, synchrotron-based X-ray diffraction (XRD) spectra in Fig. 2(d) showed that diffraction peaks of hydrogenated VO_2 shifted towards low angles, indicating the presence of slightly enlarged lattice parameters and expanded cell volumes.

Synchrotron based XANES spectra suggested that H-doping actually caused electron doping effect. Fig. 3(a) and Fig. 3(b) show the V L-edge and O K-edge XANES spectra for the pure VO_2 film and the hydrogenated samples, respectively. It can be observed that after hydrogenation, the V L-edge curves for the H-doped samples continuously shifts to lower energy direction. The V L-edge is connected with the transition from $V2p$ to $V3d$ state, thus this clear edge shift should be directly associated with the charge transfer to V atoms, resulting the valence state variation from V^{+4} to $V^{+(4-\delta)}$ state or even to V^{+3} state [12]. These V L-edge shifts are quite consistent with the XPS results as shown in Fig. 2(a). Furthermore, the electron doping effect is also clear reflected by the O K-edge spectra considering the transition from $O1s$ to $O2p$ states. From Fig. 3(b), we can observe two distinct features

including the t_{2g} and e_g peaks for the absorption curves, which directly reflect the unoccupied states [26, 27]. It is observed that after the H-doping treatment, the relative intensity ratio of the t_{2g} and e_g peaks decreased greatly. Considering the molecular orbitals of the pristine M-VO₂ phase as shown in Fig. 3(c) and Fig. 3(b), it is suggested that the doped electrons will firstly occupy the lower t_{2g} levels including the $d_{//}^*$ and π^* orbitals, resulting the Fermi level up-shift as well as producing the metallic and insulated phases. Since the states for t_{2g} levels will be gradually filled by the electron doping, the intensity of the t_{2g} absorption peak will resultantly decreased as shown in Fig. 3(b).

The above experimental characterizations thus provide structural details for a thorough theoretical investigation on the microscopic kinetics of phase transitions. First-principles simulations at the density function theory (DFT) level were applied to examine the H-doping induced geometric and electronic structure variations [28-33]. More calculated details are described in Ref. [19]. Fig. 4 shows VO₂ models with corresponding calculation results. Compared to the pure monoclinic VO₂ ($1 \times 1 \times 1$) unit cell (V₄O₈), the optimized structures of both lightly H-doped cells (HV₄O₈ or H₂V₄O₈) and saturated doping cells (H₄V₄O₈) are quite stable with negative formation energies and H-O bonds of ~ 1.00 Å [19]. H-doping induces only subtle geometric variations including slightly enhanced lattice parameters and expanded cell volumes, consistent with above characterizations and previous reports [10]. In contrast, the electronic structures were heavily affected by H-doping. All hydrogen atoms hold strong positive charges ($> 0.64 e^+$), inducing polarized electrons in V-O bonds. The energy distribution of polarized electrons can be inferred from the simulated density of states (DOS). For the pure V₄O₈ cell, valence band edge states are well separated from the conduction band in Fig. 4(d), accounting for the insulating properties of a typical semi-conductor band structure (Fig. 4(g)). With one or two H introduced into V₄O₈, the HV₄O₈ (Fig.S3 in Ref. [19]) or H₂V₄O₈ cells exhibit partially occupied conduction band-edge states. The newly occupied states are mostly $d_{//}^*$ orbitals of V atoms, suggesting that H-doping induce more d-electrons. The calculated charge densities clearly show the electron distributions and the charge transfer for the H-doped system

(Fig. S4 in Ref. [19]). The polarized d-electrons then shift up the Fermi level, and consequently cause the conduction band edge in V_4O_8 (Fig. 4(g)) to become partially occupied (Fig. 4(h)) for $H_2V_4O_8$, naturally leading to an insulator-to-metal transition. The evolution of electronic structures becomes more interesting when we add 4 H atoms into a V_4O_8 cell. The computed DOS in Fig. 4(f) shows that the polarized electrons fully occupy the original conduction band edge states in V_4O_8 . These states with lowered energies become the new valence band maximum (Fig. 4(i)), leading to an insulating ground state. The effect of varying different interstitial H sites was tested, giving similar electronic structures (Fig. S5 in Ref. [19]).

In order to unravel the actual microscopic mechanism, the gradual filling of V-3d orbitals with increasing H-concentration were simulated. A larger ($1 \times 2 \times 1$) cell of V_8O_{16} was constructed. These together with the above H-doped V_4O_8 models enabled us to examine the effect of varying doping concentration ($H_xV_8O_{16}$ with $x=0\sim 8$). The DOS features in Fig. 5(a) and Fig. S6 [19] show that increasing H-doping gradually shifted up the Fermi level to exceeding the conduction band edge state of the V-3d orbitals [19]. The V-3d occupancy was computed by integrating the corresponding DOS below the Fermi level (Fig. 5(a)). Surprisingly, the V-3d occupancy increases linearly with H-doping concentration (Fig. 5(b)). This clear relationship thus explains the phase transitions, from the insulating state (VO_2) with empty V-3d_{//}* orbitals, to the metallic states ($H_xV_8O_{16}$, $x=1\sim 7$) with un-saturated H-doping and partially-occupied conduction band edge states, and eventually to the new insulating state ($H_8V_8O_{16}$) with saturated H-doping and fully-occupied V-3d_{//}* orbitals which already became the new valence band edge. It should be noticed that the electron correlations in VO_2 system need to be accounted by many-body techniques. To test the consistency, both PBE+U and advanced HSE06 computations were conducted and exhibited nearly the same linear filling of V-3d_{//}* orbitals by H-doping (Fig.S7-8 in Ref. [19]), providing key insights for mechanism investigation.

In conclusion, the present experimental and theoretical work provides a comprehensive description of the whole dynamic process of electron-doping induced consecutive phase transitions in VO_2 crystal. We accomplished direct detection of

gradual electron occupation of the e_g/t_{2g} orbitals along with increasing H-concentration, when the formation of O–H bonds is accompanied by electrons donating from H to V and O atoms. These polarized electrons cause the partial filling of the conduction band edge, leading to metallic behavior. With saturated O–H bonds, the additional polarized electrons eventually occupy all $d_{//}$ orbitals at the previous conduction band edge, creating new valence band edge states and producing a new insulating gap. A linear relationship describing the dependence of $d_{//}$ orbital occupancy on H-doping concentration was revealed. These data and analysis provide fundamental physical insights into the H-doping induced electronic band/orbital occupancy variations and reveal the underlying mechanism of the reversible electron-doping triggered insulator-metal-insulator phase transitions. This approach should lead to the accurate control of electronic properties of this and other oxide materials in a continuously adjustable manner.

This work was partially supported by the National Basic Research Program of China (2014CB848900), the National Natural Science Foundation of China (U1432249, 11574279, 11404095), the Fundamental Research Funds for the Central Universities and the Open Research Fund of State Key Laboratory of Pulsed Power Laser Technology, Electronic Engineering Institute. The authors also acknowledge support from the Beijing Synchrotron Radiation Facility, Shanghai Synchrotron Radiation Facility and the National Synchrotron Radiation Laboratory (NSRL) of Hefei. DN and HJ acknowledge support from U.S. DOE Office of Science/Basic Energy Sciences award DE-FG02-06ER46337.

References

- [1] R. M. Wentzcovitch, W. W. Schulz, and P. B. Allen, *Phys. Rev. Lett.* **72**, 3389 (1994).
- [2] M. M. Qazilbash, K. S. Burch, D. Whisler, D. Shrekenhamer, B. G. Chae, H. T. Kim, and D. N. Basov, *Phys. Rev. B* **74**, 205118 (2006).

- [3] H. T. Kim, Y. W. Lee, B. J. Kim, B. G. Chae, S. J. Yun, K. Y. Kang, K. J. Han, K. J. Yee, and Y. S. Lim, *Phys. Rev. Lett.* **97**, 266401 (2006).
- [4] J. I. Sohn, H. J. Joo, D. Ahn, H. H. Lee, A. E. Porter, K. Kim, D. J. Kang, and M. E. Welland, *Nano Lett.* **9**, 3392 (2009).
- [5] M. M. Qazilbash et al., *Science* **318**, 1750 (2007).
- [6] S. Biermann, A. Poteryaev, A. I. Lichtenstein, and A. Georges, *Phys. Rev. Lett.* **94**, 026404 (2005).
- [7] T. C. Koethe, Z. Hu, M. W. Haverkort, C. Schüßler-Langeheine, F. Venturini, N. B. Brookes, O. Tjernberg, W. Reichelt, H. H. Hsieh, H.-J. Lin, C. T. Chen, and L. H. Tjeng, *Phys. Rev. Lett.* **97**, 116402 (2006).
- [8] X. Tan, T. Yao, R. Long, Z. Sun, Y. Feng, H. Cheng, X. Yuan, W. Zhang, Q. Liu, C. Wu, Y. Xie, and S. Wei, *Sci. Rep.* **2**, 466 (2012).
- [9] Y. Wu, L. Fan, W. Huang, S. Chen, S. Chen, F. Chen, C. Zou, and Z. Wu, *Phys. Chem. Chem. Phys.* **16**, 17705 (2014).
- [10] Y. Filinchuk, N. A. Tumanov, V. Ban, H. Ji, J. Wei, M. W. Swift, A. H. Nevidomskyy, and D. Natelson, *J. Am. Chem. Soc.* **136**, 8100 (2014).
- [11] J. Lin, H. Ji, M. W. Swift, W. J. Hardy, Z. Peng, X. Fan, A. H. Nevidomskyy, J. M. Tour, and D. Natelson, *Nano Lett.* **14**, 5445 (2014).
- [12] J. Wei, H. Ji, W. Guo, A. H. Nevidomskyy, and D. Natelson, *Nat. Nanotechnol.* **7**, 357 (2012).
- [13] K. H. Warnick, B. Wang, S. T. Pantelides, *Appl. Phys. Lett.* **104**, 101913 (2013).
- [14] W.K. Yin, Y. Qin, W. B. Fowler, M. Stavola, L.A. Boatner, *J. Phys.: Condens. Matter* **28**, 395401 (2016)
- [15] H.J. Yoon, M. Choi, T.W. Lim, H. Kwon, K. Ihm, J. K. Kim, S.Y. Choi, J. Son, *Nat. Mater.* **15**, 1113 (2016)
- [16] N. B. Aetukuri, A. X. Gray, M. Drouard, M. Cossale, L. Gao, A. H. Reid, R. Kukreja, H. Ohldag, C. A. Jenkins, E. Arenholz, K. P. Roche, H. A. Durr, M. G. Samant, and S. S. P. Parkin, *Nat. Phys.* **9**, 661 (2013).
- [17] John B. Goodenough, *J. Solid State Chem.* **3**, 490 (1971).

- [18] L. L. Fan, S. Chen, Y. F. Wu, F. H. Chen, W. S. Chu, X. Chen, C. W. Zou, and Z. Y. Wu, *Appl. Phys. Lett.* **103**, 131914 (2013).
- [19] See Supplemental Material at <http://www.aps.org/> for detailed information on the experimental and DFT calculated process, electric measurement and XPS curve fitting results..
- [20] M. Demeter, M. Neumann, and W. Reichelt, *Surf. Sci.* **454**, 41 (2000)
- [21] G. Silversmit, D. Depla, H. Poelman, G. B. Marin, and R. De Gryse, *J. Electron Spectros. Relat. Phenomena* **135**, 167 (2004)
- [22] S. Kačičulis, G. Mattogno, A. Napoli, E. Bemporad, F. Ferrari, A. Montenero, and G. Gnappi, *J. Electron Spectros. Relat. Phenomena* **95**, 61 (1998).
- [23] G. Philippin, J. Delhalle, and Z. Mekhalif, *Appl. Surf. Sci.* **212**, 530 (2003).
- [24] M. M. Qazilbash, A. A. Schafgans, K. S. Burch, S. J. Yun, B. G. Chae, B. J. Kim, H. T. Kim, and D. N. Basov, *Phys. Rev.B* **77**, 115121 (2008)
- [25] T. J. Huffman, P. Xu, A. J. Hollingshad, M. M. Qazilbash, L. Wang, R. A. Lukaszew, S. Kittiwatanakul, J. Lu, and S. A. Wolf, *Phys. Rev.B* **91**, 205140 (2015)
- [26] S. Kumar, J. P. Strachan, M. D. Pickett, A. Bratkovsky, Y. Nishi, R. S. Williams, *Adv. Mater.* **26**, 7505 (2014)
- [27] A. X. Gray, J. Jeong, N. P. Aetukuri, P. Granitzka, Z. Chen, R. Kukreja, D. Higley, T. Chase, A. H. Reid, H. Ohldag, M. A. Marcus, A. Scholl, A. T. Young, A. Doran, C. A. Jenkins, P. Shafer, E. Arenholz, M. G. Samant, S. S. P. Parkin, H. A. Dürr, *Phys. Rev.Lett.* **116**, 116403 (2016)
- [28] G. Kresse, D. Joubert, *Phys. Rev. B* **59**, 1758 (1999)
- [29] J. P. Perdew, K. Burke, M. Ernzerhof M., *Phys. Rev. Lett.* **77**, 3865 (1996).
- [30] V. Eyert, *Phys. Rev. Lett.* **107**, 016401 (2011).
- [31] J. Heyd, G.E.Scuseria, M. Ernzerhof M., *J. Chem. Phys.* **124**, 219906 (2006)
- [32] G. Kresse, J. Furthmuller, *Phys. Rev. B* **54**, 11169 (1996)
- [33] V. I. Anisimov, F. Aryasetiawan, A. I. Lichtenstein, *J. Phys. Condens. Matter*, **9**, 767(1997)

Figures and Captions

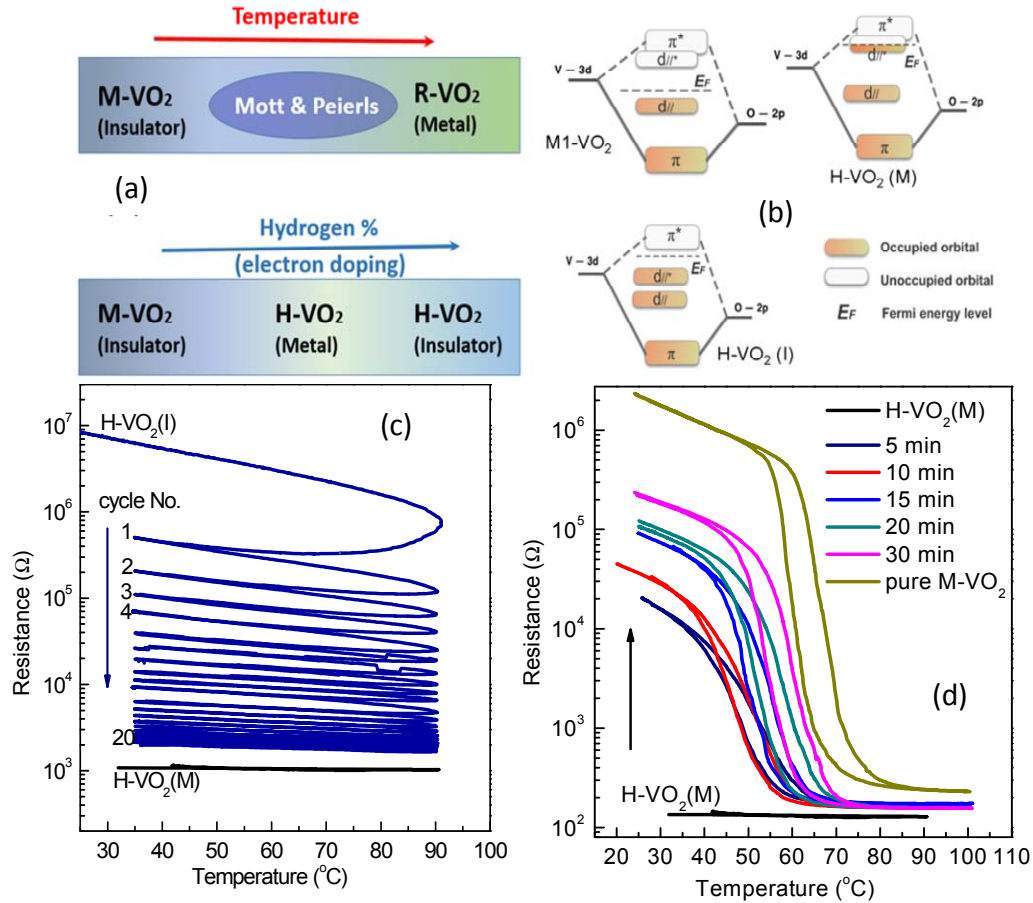


FIG. 1 (a) Scheme for the phase transitions induced by temperature and electron doping. For the hydrogenation effect, two hydrogen-doped VO_2 phases exist, which show insulating ($\text{H-VO}_2(\text{I})$) and metallic ($\text{H-VO}_2(\text{M})$) states, respectively; (b) Molecular orbitals and band diagrams for monoclinic VO_2 insulator and H-doped VO_2 in its metallic/insulating phase; (c) R-T curves for insulating $\text{H-VO}_2(\text{I})$ and metallic $\text{H-VO}_2(\text{M})$ film samples. During a series of 20 heating/cooling cycles in vacuum over the range of 35°C to 90°C at a constant ramp rate of 0.4K/s , the R-T curve for the $\text{H-VO}_2(\text{I})$ insulator film shows a gradual transformation to the metallic $\text{H-VO}_2(\text{M})$ state. (d) The metallic $\text{H-VO}_2(\text{M})$ converts to monoclinic insulating state after

baking in air at 180°C. After the 30min treatment, it trend to recovery to the initial M-VO₂ state.

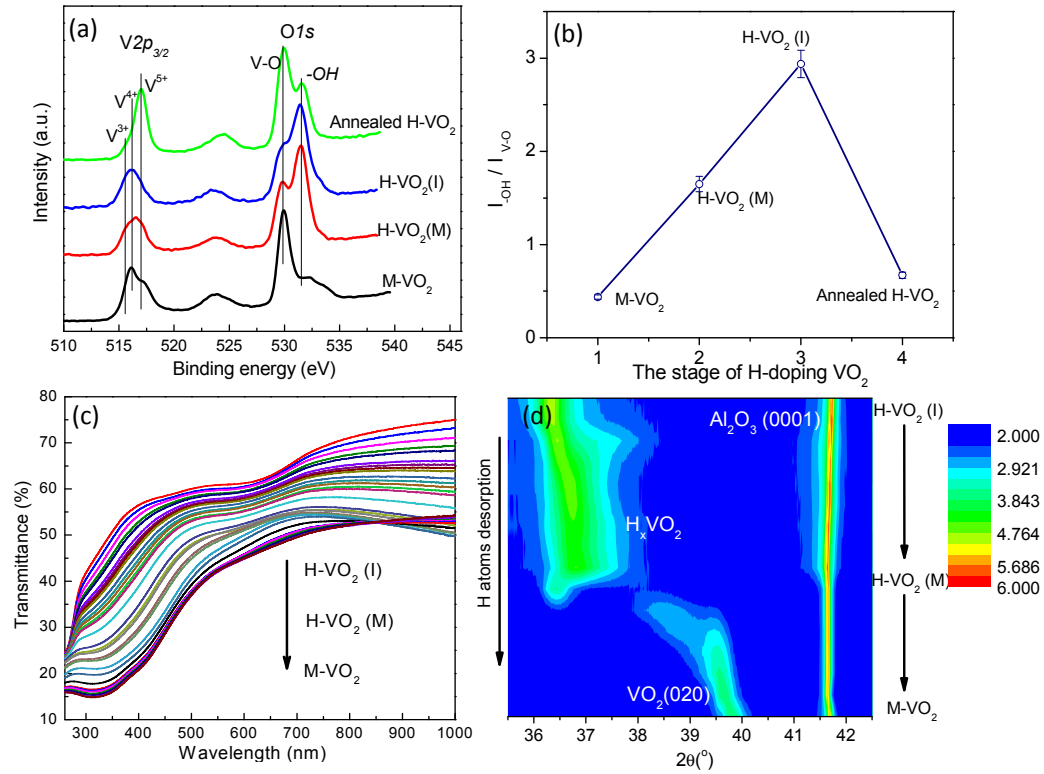


FIG. 2 (a) XPS spectra for VO₂ films: the as-prepared M-VO₂ film, H-VO₂ (M), H-VO₂ (I) and annealed H-doped VO₂ film, showing clear differences between the V2p and O1s peaks. (b) The intensity ratio between the -OH peak and V-O peak; (c) The UV-Vis spectra for H-doped films during phase transitions. (d) The crystal lattice variations during the hydrogenation process.

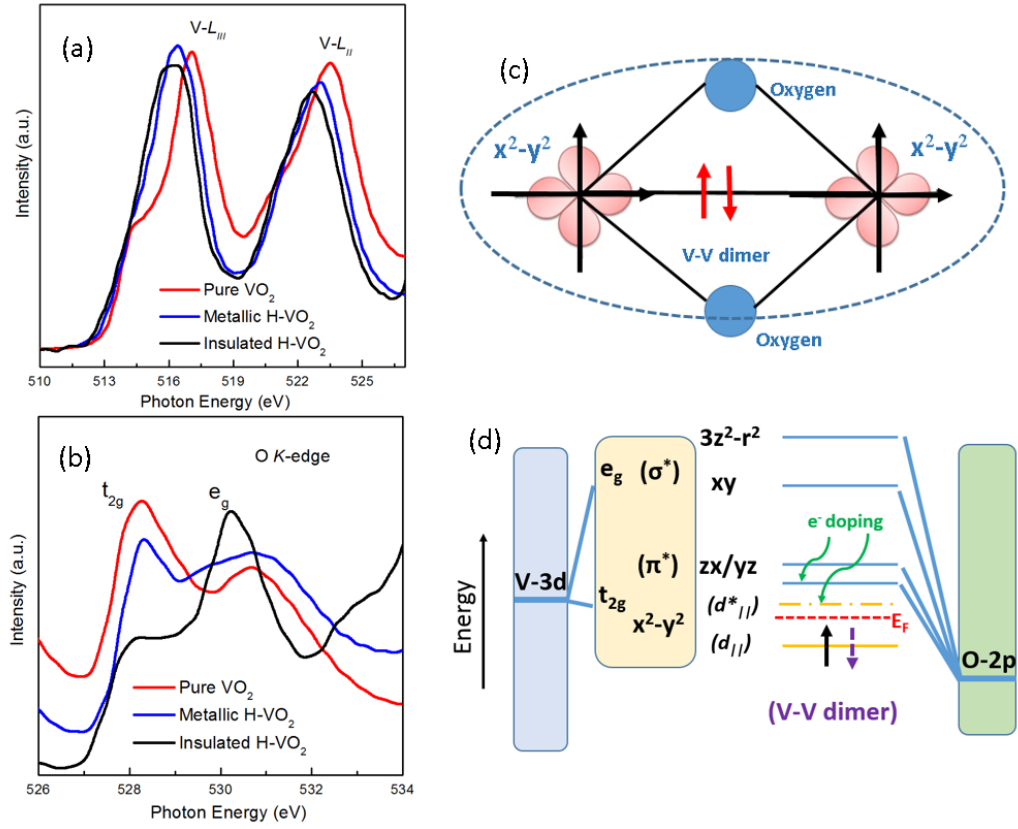


FIG. 3 (a) The synchrotron based V L-edge XANES measurements for the samples before and after hydrogenation. It can be observed that the V L-edge shifts to lower energy direction due to the H-doping, showing the charge transfer effect from the H dopants; (b) The typical O K-edge XANES measurements for the samples before and after hydrogenation. (c) The molecular orbitals of the pristine M-VO₂ phase with the V-V dimers and (d) electron orbitals occupancy during the electron doping process.

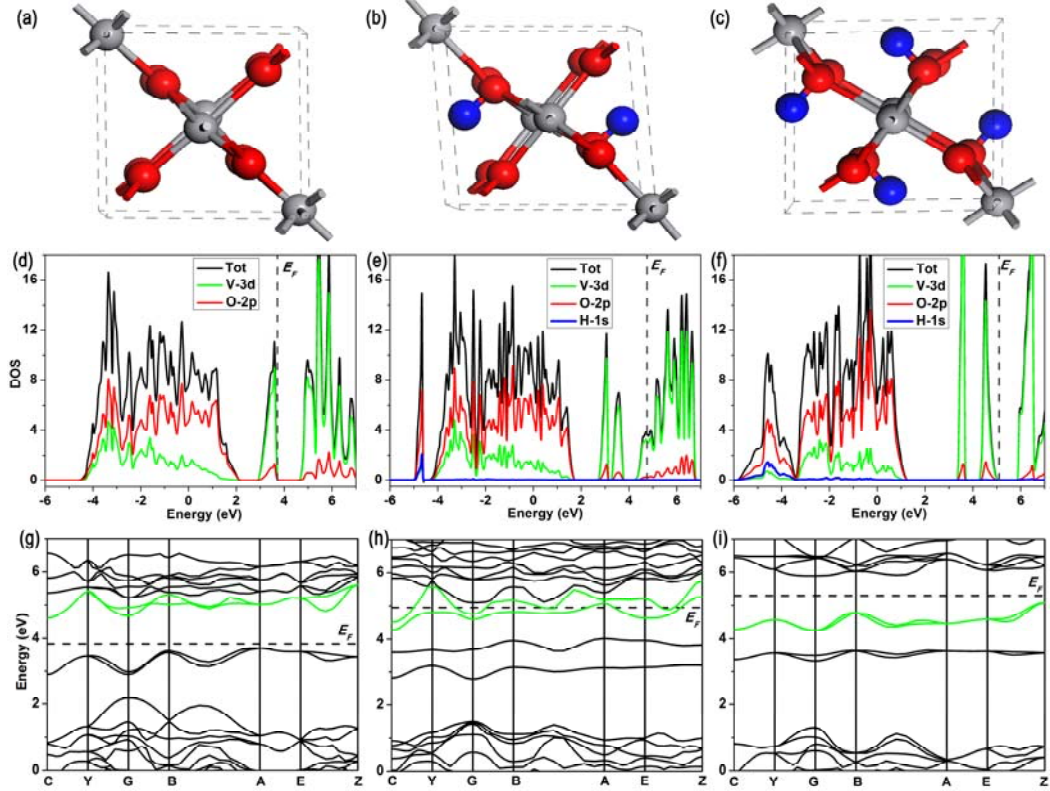


FIG. 4 Optimized atomic structures (top panel), density of states (DOS: middle panel), band structures (bottom panel) of the pure monoclinic VO_2 unit cell (V_4O_8) and H-doped cells ($H_xV_4O_8$ with $x=2, 4$). (a), (b), (c) are the crystal structures of V_4O_8 , $H_2V_4O_8$, and $H_4V_4O_8$, respectively. The red, grey, and blue balls represent O, V and H atoms, respectively. (d), (e), (f) are the DOS of V_4O_8 , $H_2V_4O_8$ and $H_4V_4O_8$, respectively, where the Fermi level E_F is marked with dashed lines. (g), (h), (i) are the band structures of V_4O_8 , $H_2V_4O_8$ and $H_4V_4O_8$, respectively.

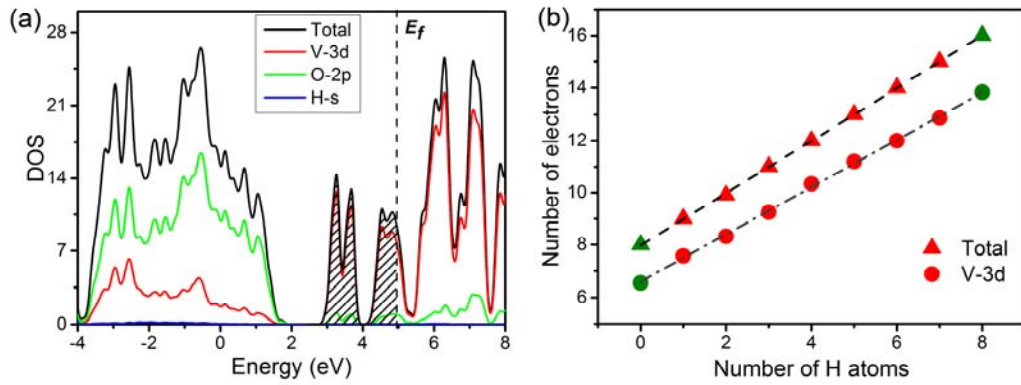


FIG. 5 (a) The DOS of $H_3V_4O_8$, in which the shaded areas represent occupancy of the conduction band edge state, corresponding to DOS below the Fermi level E_F . (b) The electron occupancy of the total and V-3d DOS (computed by integrating the shaded areas) as a function of H-doping concentration.